PCCP

Accepted Manuscript

ROYAL SOCIETY OF CHEMISTRY

www.rsc.org/pccp

Physical Chemistry Chemical Physics RSCPublishing

COMMUNICATION

Sub-10 nm Monodisperse PbS Cubes by Post-Synthesis Shape Engineering

Cite this: DOI: 10.1039/xoxxoooooox

Haitao Zhang,[a]† Jun Yang,[a] Tobias Hanrath,[b] and Frank W. Wise [a]

Received ooth January 2012,
Accepted ooth January 2012

DOI: 10.1039/xoxxoooooox

www.rsc.org/

Abstract: Sub-10 nm monodisperse PbS cubes are synthesized by reacting quasi-spherical PbS nanocrystals with $(NH_4)_2S$. This reaction shapes the quasi-spheres into cubes *via* preferential growth of the (111) facets. A four-band envelope function calculation of the energy levels accounts well for the measured absorption spectra. Initial studies show that PbS cubes can organize into simple square superlattices with short ligands.

Lead chalcogenide colloidal nanocrystals (NCs) attract much attention due to their excellent size-tunability across the near-infrared (NIR) region.[1-4] Colloidal synthesis provides precise shape control and lead chalcogenide colloidal NCs of a variety of shapes have been obtained.[5-12] Cubic-shape NCs are especially desirable for thin film applications because of their advantages of strong inter-particle coupling and low void volume in close packed assemblies.[12-16]Although theoretical calculations predict that a cube is the thermodynamically stable shape of lead chalcogenide NCs,[17-19] only relatively large size (>10 nm) cubic lead chalcogenide NCs have been synthesized.[8, 10-12] Small size (< 10 nm) lead chalcogenide NCs tend to adopt a quasi-spherical shape to minimize the surface energy and thus, it is difficult to obtain small cubic NCs through conventional synthesis.

Kinetically, formation of cubic lead chalcogenide NCs (which have the rock salt crystal structure) requires fast growth of the high surface energy (111) facets to yield the crystal shape defined by low surface energy (100) facets. We report here a novel method that can shape quasi-spherical PbS NCs into cubes by selective growth of the (111) facets, through chemical treatment of quasi-spherical PbS NCs by $(NH_4)_2S$. Optical absorption spectra of the PbS cubes are modelled by a four-band envelope function calculation of the energy levels. The self-assembly of these sub-10 nm PbS cubes exhibits an interesting dependence on the size of surfactants. When smaller ligands such as octylamine are used, the NCs assemble into simple square superlattices. These assemblies are further evidence of the cubic character of the NC shape, and they offer great promise for future applications.

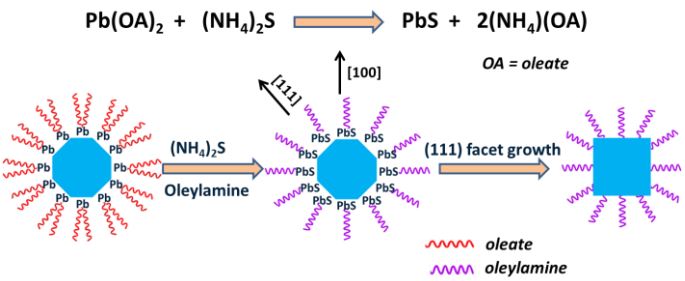

Figure 1. Schematic of PbS NCs shape transformation from quasi-sphere to cube by reacting with $(NH_4)_2S$.

Synthesis of cubic PbS NCs was carried out by reacting quasi-spherical PbS NCs with anhydrous $(NH_4)_2S$ in a solution of primary amine such as oleylamine. Oleylamine is a good organic solvent of $(NH_4)_2S$[20] and has been used as a surfactant ligand in the synthesis of large size (> 10 nm) cubic PbS NCs.[8] In a typical reaction, 15 mg of as-synthesized quasi-spherical PbS NCs in 4 mL hexanes was combined with 0.12 mmol $(NH_4)_2S$ in 4 mL oleylamine. For NCs smaller than 5 nm diameter, a small amount of oleic acid (0.2 mL) was added to help stabilize NCs. The reaction was allowed to proceed for 30 minutes at room temperature before adding acetone to precipitate out the NC products.

$(NH_4)_2S$ can react with the lead oleate complexes on PbS NC surfaces and convert lead oleate into PbS (Figure 1). Our previous study[21] has shown that when this reaction is performed in an alcohol solution of excess $(NH_4)_2S$ without the presence of a secondary surfactant ligand oleylamine, NCs are directly connected to each other by the newly-formed Pb-S bonds due to the loss of surfactant ligands. In this work, the use of a limited amount of $(NH_4)_2S$ with copious oleylamine ligands prevents the connection of NCs and stabilizes the NCs in colloidal solution.

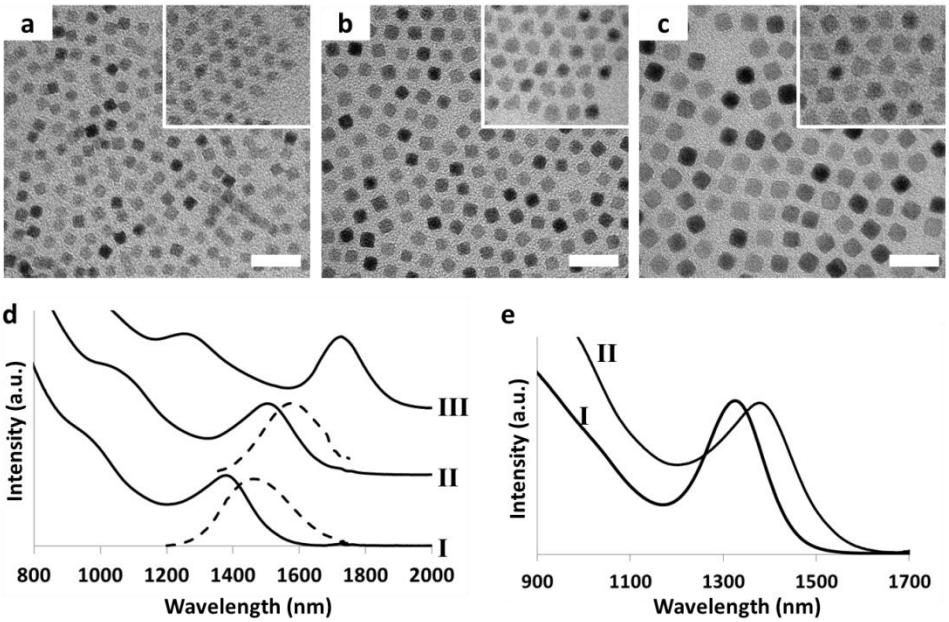

Figure 2. a-**c**) TEM images of cubic PbS NCs of different sizes (edge): **a**, 4.6±0.3 nm; **b**, 5.5±0.3 nm; **c**, 7.0±0.4 nm. Insets of **a**-**c** are TEM images of the corresponding starting quasi-spherical PbS NCs with sizes (diameter): **a**, 5.2±0.4 nm; **b**, 5.9±0.4 nm; **c**, 7.3±0.4 nm. The edges of cubes are slightly shorter than the diameters of the corresponding starting quasi-spheres, while the volumes of cubes are larger than those of quasi-spheres if we assume the latter have spherical shape: V_{cube}/V_{sphere} = 1.3/1(**a**), 1.5/1 (**b**), 1.7/1 (**c**). These observations are consistent with the proposed shape transformation mechanism (Figure 1). The inset and main pictures have the same magnification. Scale bar: 20 nm. **d**) Optical absorption (solid) and photoluminescence (dashed) spectra of cubic PbS NCs of different sizes: **I**, 4.6 nm; **II**, 5.5 nm; **III**, 7.0 nm. **e**) Optical absorption spectra of 4.6 nm cubic PbS NCs (**II**) and their starting quasi-spherical PbS NCs (**I**).

After the reaction, the NC products can be re-dispersed in nonpolar solvents such as hexanes or toluene. Transmission electron microscope (TEM) images reveal the cubic shape of the final NC products, which is clearly distinct from the quasi-spherical shape of the starting NCs (Figure 2a-c). We did not observe such a shape transformation in a control experiment, which consisted of stirring quasi-spherical PbS NCs in oleylamine without adding $(NH_4)_2S$ (*Electronic Supplementary Information*, *Figure* S5). Thus, the formation of cubic NCs must be a result of the reaction of $(NH_4)_2S$ with the quasi-spherical PbS NCs.

We tentatively explain the formation of the cubic PbS NCs based on the mechanism illustrated in Figure 1. It is well-accepted that PbS NCs passivated with oleate ligands have a Pb-rich (compared to S^{2-}) surface of $Pb^{2+}(OA^-)_x(S^{2-})_{1-x/2}$ ($0<x<2$) based on stoichiometry. The excess Pb^{2+} should coordinate to both OA^- and S^{2-} anions. For clarity, we can simplify the structure of PbS NCs as a layer of $Pb(OA)_2$ that resides on the surface of stoichiometric PbS cores (Figure 1). The reaction of $(NH_4)_2S$ with quasi-spherical PbS NCs converts surface lead oleate complexes into PbS. The newly-formed PbS is redistributed on the NC surface crystal lattice *via* facet growth. Compared to the temperature (> 90 ^oC) used in the synthesis of the starting quasi-spherical NCs, our synthesis is performed at a lower temperature (room temperature), which suppresses the growth of the less-reactive (100) facets. This leads to preferential growth of the more reactive (111) facets, which reshapes the quasi-spherical NCs into cubes terminated by (100) facets. We expect that this shape transformation strategy is applicable to the PbS NCs passivated with other surfactant ligands, as long as a) NC surface has enough excess Pb^{2+} (compared to S^{2-}), and b) Pb^{2+}-surfactant ligand complexes have suitable reactivity with $(NH_4)_2S$ or other sufide sources.

The optical absorption spectra of the cubic PbS NCs reveal well-resolved excitonic absorption peaks, with full-width at half-maximum (FWHM) of ~150 nm (Figure 2d), comparable to the reported results of monodisperse quasi-spherical PbS NCs. The absorption peaks of the cubic PbS NCs are red-shifted compared to those of the starting quasi-spherical NCs (Figure 2e). For 4.6-nm cubic NCs, this red-shift is about 50 nm. Such a red-shift is consistent with our proposed mechanism: the volume of the NCs increases slightly after reacting with $(NH_4)_2S$, as described in Figure 1. The room-temperature photoluminescence (PL) of the cubic PbS NCs has a small Stokes shift (Figure 2d), with fluorescence quantum yield of 3-5% (for details see the *Electronic Supplementary Information*).[22]

The four-band envelope function theory accounts well for the electronic states of quasi-spherical PbS NCs.[23] Here we employ the same approach to model the electronic states of the cubic PbS NCs (for details see the *Electronic Supplementary Information*). The coupling between the highest valence band and the conduction bands as well as coupling between the lowest conduction band and the valence bands are included in a second-order perturbation approximation. Spin-orbit interaction is also accounted for in the model. The boundary condition is assumed to be that of an infinite well. The inter-valley coupling, band anisotropy, coulomb interaction and exchange interaction are neglected. The 4-band Hamiltonian reads:

$$H_0(\boldsymbol{k}) = \begin{bmatrix} \left(\frac{E_g}{2} + \frac{\hbar^2\boldsymbol{k}^2}{2m^-}\right)\boldsymbol{I} & \frac{\hbar P}{m}\boldsymbol{k}\cdot\boldsymbol{\sigma} \\ \frac{\hbar P}{m}\boldsymbol{k}\cdot\boldsymbol{\sigma} & -\left(\frac{E_g}{2} + \frac{\hbar^2\boldsymbol{k}^2}{2m^+}\right)\boldsymbol{I} \end{bmatrix} \quad (1)$$

which is a 4×4 matrix, where P is the Kane momentum-matrix element between the conduction and balance band-edge Bloch functions; m^- and m^+ are the band-edge effective masses for the conduction band and valence band respectively; m is the free electron mass; $\boldsymbol{\sigma}$ is the Pauli matrix. All parameters in the calculation use the same values as in ref. 23.

The quantum confined levels are obtained by solving the envelope function equation with imposed boundary condition:

$$H_0(-i\nabla)\mathcal{F}(\boldsymbol{r}) = E\mathcal{F}(\boldsymbol{r}) \quad (2)$$

$$\mathcal{F}(r_i = 0, L) = 0\,, \qquad \text{for } i = x, y, z \quad (3)$$

Here the envelope wavefunction $\mathcal{F}(\boldsymbol{r})$ is a four-component vector $[F_j(\boldsymbol{r})]$, $j = 1 \ldots 4$. It is not clear whether an analytic solution exists at all. However, it can always be expanded in a set of basic functions that satisfy the boundary conditions

$$\mathcal{F}_j(\boldsymbol{r}) = \sum_{\alpha,\beta,\gamma>0} A_{j,\alpha,\beta,\gamma} \sin(\frac{\alpha\pi x}{L}) \sin(\frac{\beta\pi y}{L}) \sin(\frac{\gamma\pi z}{L}) \quad (4)$$

where α, β, γ are all integers. It is also expected that, for low energy states, there will be very small contributions from basis states with large momentum (large α, β, γ). Therefore, to calculate the energies of states close to the band edge, one only needs to account for a limited number of basis functions to obtain a satisfactory solution. Here we use a simple cutoff number N=8, and count only the basis functions with $1 \le \alpha, \beta, \gamma \le N$. This corresponds to a total of $4 \times N^3$ basis functions. By inserting this form of the wavefunction into the Schrödinger Equation (2), and using the orthogonal relations we obtain a secular equation for quantum confined energy E (for full equations see the *Electronic Supplementary Information*).

The calculated energy levels are shown in Figure 3a. It can be seen that the degeneracy of states is very similar to what one would expect from a simple particle in a box model. Therefore we use the notation (n_1, n_2, n_3) to label states. The first electron state, labelled as $(111)_e$, is 2-fold spin degenerate (in addition to the degeneracy due to equivalent L valleys). The next group of states, labeled as $(112)_e$, is 6-fold degenerate. The degeneracy is slightly split due to spin-orbit interaction, into four states with lower energy, and two states with higher energy. The third group $(122)_e$, is also 6 fold degenerate, again split by spin-orbit coupling.

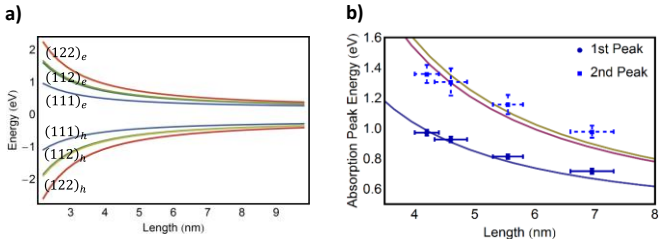

Figure 3. **a**) Energies for the first 12 states for electron and hole as a function of length for PbS cube. **b**) Calculated transition energy from $(111)_h$ to $(111)_e$ and $(112)_h$ to $(112)_e$ compared with measured center of the first and second absorption peaks. The error bar for length is the standard deviation of cube length measured in TEM. The error bar for peak energy is estimated as HWHM of the relevant 2nd derivative of the peak in absorption spectrum.

Figure 3b compares the calculated first peak position (transition from $(111)_h$ to $(111)_e$) and second peak position (transition from $(112)_h$ to $(112)_e$) with peaks in the measured absorption spectrum. The peak positions were determined from the second derivative of the absorption spectra. Transitions from $(111)_h$ to $(112)_e$ and $(112)_h$ to $(111)_e$ are parity-forbidden. The theory agrees with the experimental data reasonably well. We also find a simple analytic expression $E_g = 0.41 + \frac{1}{0.149a + 0.061a^2}$ to fit our calculation result for future reference (here a is the edge length of the cube).

As mentioned above, a major motivation to synthesize cubic NCs derives from the expected properties of the corresponding NC solids. The self-assembly of cubic PbS NCs in thin films is significantly influenced by their shape. Figure 4 shows the 2-theta x-ray diffraction (XRD) patterns of the thin films (ca. 50 nm thick) of cubic and quasi-spherical PbS NCs that were prepared by drop-casting on quartz substrate. The quasi-spherical NCs exhibit a XRD pattern with preferential alignment along [220] direction. In contrast, films of the cubic NCs produce only the (200) reflection. The ratio of the (200) to (111) reflection intensities provides a measure of the preferred orientation of the PbS crystal relative to the substrate.[11] The fact that our PbS NC products exhibit exclusively the (200) reflection in the XRD pattern indicates a strong preference of [100] alignment normal to the plane of the film, consistent with alignment of flat facets of the nanocube with the plane of the substrate.

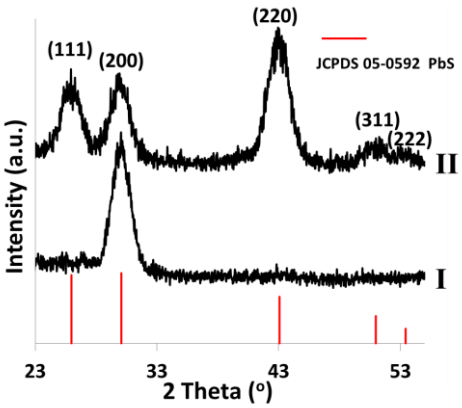

Figure 4. XRD patterns of 4.6 nm cubic (**I**) and the corresponding starting quasi-spherical (**II**) PbS NC thin films. The NC thin films (with ca. 50 nm thickness) were prepared by drop casting 1mg/mL NC solution in octane/hexanes (5:1 in volume) on quartz substrate.

The self-assembly of cubic PbS NCs exhibits strong dependence on the size of the surfactant ligands. Cubic NCs are highly desirable in NC thin-film applications because of their potential to be assembled into close-packed simple cubic superlattices, which will have strong inter-NC coupling. We find that the cubic PbS NCs with oleylamine ligands tend to form disordered aggregates (sub-5 nm NCs) or hexagonal superlattices (Figure 2). It seems like these small PbS cubes behave more like spheres, and do not interact through their cubic shape in the presence of the long oleylamine ligands (which have 18 carbon atoms). This is consistent with self-assembly trends of colloidal nanocubes previously reported.[24] When we use the shorter octylamine ligand (8 carbon atoms) instead of oleylamine in the synthesis (thus the cubic PbS NCs being passivated by octylamine), PbS cubes readily assemble into simple square superlattices (Figure 5).

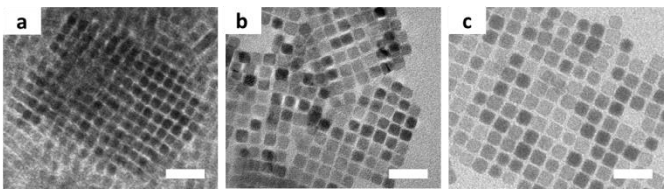

Figure 5. TEM images of the simple square superlattice assembled by different sizes of cubic PbS NCs: **a**, 4.6 nm; **b**, 5.5 nm; **c**, 7.0 nm. These cubic PbS nanocrystals were synthesized in octylamine solution. Scale bar:20 nm.

Conclusions

In conclusion, we report the synthesis of sub-10 nm monodisperse cubic PbS NCs. Cubic PbS NCs are formed by reacting quasi-spherical PbS NCs with $(NH_4)_2S$. Such a shape engineering strategy is novel in colloidal NC synthesis. A four-band envelope function calculation of the electron energies accounts well for the measured absorption spectra. The cubic shape significantly influences self-assembly of the NCs. Initial studies show that the cubic PbS NCs organize into simple square superlattices with short ligands such as octylamine. These superlattices provide a promising model system for inter-NC coupling studies as well as for NC thin film applications.

Acknowledges

Research was supported by the U.S. Department of Energy, Office of Basic Energy Sciences, Division of Materials Sciences and Engineering, under Award DESC0006647. Material characterization was performed in the Cornell Center for Materials Research (CCMR), with funding from the Materials Research Science and Engineering Center program of the National Science Foundation (cooperative agreement DMR 1120296).

Notes and references

[a] School of Applied and Engineering Physics, [b] School of Chemical and Biomolecular Engineering, Cornell University, Ithaca, NY 14853.

† Address correspondence to hz244@cornell.edu.

Electronic Supplementary Information (ESI) available: Materials, nanocrystal synthesis, characterization techniques described in the text, details of NC energy level calculations, and additional TEM images. See DOI: 10.1039/c000000x/

References

1 F. W. Wise, *Accounts Chem. Res.*, 2000, **33**, 773-780.
2 L. Sun, J. J. Choi, D. Stachnik, A. C. Bartnik, B.-R. Hyun, G. G. Malliaras, T. Hanrath and F. W. Wise, *Nat. Nano*. 2012, **7**, 369-373.
3 A. H. Ip, S. M. Thon, S. Hoogland, O. Voznyy, D. Zhitomirsky, R. Debnath, L. Levina, L. R. Rollny, G. H. Carey, A. Fischer, K. W. Kemp, I. J. Kramer, Z. Ning, A. J. Labelle, K. W. Chou, A. Amassian and E. H. Sargent, *Nat. Nano*, 2012, **7**, 577-582.
4 Y. Liu, J. Tolentino, M. Gibbs, R. Ihly, C. L. Perkins, Y. Liu, N. Crawford, J. C. Hemminger and M. Law, *Nano Lett.*, 2013, **13**, 1578-1587
5 M. A. Hines and G. D. Scholes, *Adv. Mater.*, 2003, **15**, 1844-1849.
6 K.-S. Cho, D. V. Talapin, W. Gaschler and C. B. Murray, *J. Am. Chem. Soc.*, 2005, **127**, 7140-7147.
7 W.-k. Koh, A. C. Bartnik, F. W. Wise and C. B. Murray, *J. Am. Chem. Soc.*, **132**, 3909-3913.
8 J. Joo, H. B. Na, T. Yu, J. H. Yu, Y. W. Kim, F. Wu, J. Z. Zhang and T. Hyeon, *J. Am. Chem. Soc.*, 2003, **125**, 11100-11105.
9 C. B. Murray, S. Sun, W. Gaschler, H. Doyle, T. A. Betley and C. R. Kagan, *IBM J. Res. Dev.*, 2001, **45**, 47.
10 H. Li, D. Chen, L. Li, F. Tang, L. Zhang and J. Ren, *CrystEngComm*, 2010, **12**, 1127-1133.
11 W. J. Baumgardner, Z. Quan, J. Fang and T. Hanrath, *Nanoscale*, 2012, **4**, 3625-3628.
12 W.-k. Koh, S. R. Saudari, A. T. Fafarman, C. R. Kagan and C. B. Murray, *Nano Lett.*, 2011, **11**, 4764-4767.
13 P. Liljeroth, K. Overgaag, A. Urbieta, B. Grandidier, S. G. Hickey and D. l. Vanmaekelbergh, *Phys. Rev. Lett.*, 2006, **97**, 096803.
14 E. Kalesaki, C. Delerue, C. Morais Smith, W. Beugeling, G. Allan and D. Vanmaekelbergh, *Phys. Rev. X*, 2014, **4**, 011010.
15 J. Gong, G. Li and Z. Tang, *Nano Today*, 2012, **7**, 564-585.
16 Y. Gao and Z. Tang, *Small*, 2011, **7**, 2133-2146.
17 C. R. Bealing, W. J. Baumgardner, J. J. Choi, T. Hanrath and R. G. Hennig, *ACS Nano*, 2012, **6**, 2118-2127.
18 C. Fang, M. A. van Huis, D. l. Vanmaekelbergh and H. W. Zandbergen, *ACS Nano*, 2009, **4**, 211-218.
19 M. Argeri, A. Fraccarollo, F. Grassi, L. Marchese and M. Cossi, *J. Phys. Chem. C*, 2011, **115**, 11382-11389.
20 H. Zhang, B.-R. Hyun, F. W. Wise and R. D. Robinson, *Nano Lett.*, 2012, **12**, 5856-5860.
21 H. Zhang, B. Hu, L. Sun, R. Hovden, F. W. Wise, D. A. Muller and R. D. Robinson, *Nano Lett.*, 2011, **11**, 5356-5361.
22 J. C. de Mello, H. F. Wittmann and R. H. Friend, *Adv. Mater.*, 1997, **9**, 230-232.
23 I. Kang and F. W. Wise, *J. Opt. Soc. Am. B*, 1997, **14**, 1632-1646.
24 Y. Zhang, F. Lu, D. van der Lelie and O. Gang, *Phys. Rev. Lett.*, 2011, **107**, 135701.

